Visible-to-Telecom Quantum Frequency Conversion of Light from a Single Quantum Emitter

Sebastian Zaske,[1] Andreas Lenhard,[1] Christian A. Keßler,[2] Jan Kettler,[2] Christian Hepp,[1] Carsten Arend,[1] Roland Albrecht,[1] Wolfgang-Michael Schulz,[2] Michael Jetter,[2] Peter Michler,[2] and Christoph Becher[1,*]

[1]*Fachrichtung 7.2 (Experimentalphysik), Universität des Saarlandes, Campus E2.6, 66123 Saarbrücken, Germany*

[2]*Institut für Halbleiteroptik und Funktionelle Grenzflächen and Research Center SCoPE, Universität Stuttgart, 70569 Stuttgart, Germany*

(Received 18 June 2012; published 4 October 2012)

We demonstrate efficient (>30%) quantum frequency conversion of visible single photons (711 nm) emitted by a quantum dot to a telecom wavelength (1313 nm). Analysis of the first- and second-order coherence before and after wavelength conversion clearly proves that pivotal properties, such as the coherence time and photon antibunching, are fully conserved during the frequency translation process. Our findings underline the great potential of single photon sources on demand in combination with quantum frequency conversion as a promising technique that may pave the way for a number of new applications in quantum technology.

DOI: 10.1103/PhysRevLett.109.147404 PACS numbers: 78.67.Hc, 42.50.Ex, 42.65.Ky, 78.55.−m

Quantum frequency conversion (QFC), a nonlinear optical process in which the frequency of a quantum light field is altered while conserving its nonclassical correlations, was first demonstrated 20 years ago [1]. The majority of QFC experiments [2–7] that have been performed so far focused on quantum frequency up-conversion to efficiently translate telecom light to visible wavelengths. Here it was experimentally proven that photon entanglement [4] and antibunching of light from a single quantum emitter [5,8] are not destroyed by this nonlinear process. Very recently, also Hong-Ou-Mandel-type two-photon interference was demonstrated before and after frequency up-conversion [8]. In contrast to up-conversion, interest in the reverse process, quantum frequency down-conversion (QFDC), began to grow only in recent years [9–16]. Two seminal experiments recently demonstrated QFDC of heralded single photons and entangled photons either retrieved from a quantum memory [14] or produced via spontaneous parametric down-conversion [16].

QFC is an enabling technology for many applications in the field of quantum communication: for the realization of quantum repeaters [17–19], different system components such as quantum memories and quantum processors have to be linked by long-haul quantum networks requiring telecom photons as low-loss flying qubits [9,11,13,20]. Although there has been impressive progress in the realization of telecom-wavelength quantum memories [21,22], most of the current implementations of efficient quantum memories work in the visible spectral range [23]. Thus, bridging the gap between the wavelengths of system components and flying qubits requires efficient and faithful QFC of single photons. Furthermore, QFDC allows for the realization of a wavelength tunable on-demand single photon source at telecom wavelengths by combining a quantum emitter in the near-infrared with QFDC and the implementation of single-photon wavelength division multiplexing for quantum key distribution [24].

In this Letter we present, as a proof-of-principle experiment, QFDC of visible single photons using difference frequency generation (DFG) in a Zn-doped periodically poled lithium niobate (Zn:PPLN) waveguide (WG) [25]. The visible photons in our experiment are emitted by a single quantum emitter, namely, an InP/GaInP quantum dot (QD), and no heralding is used. The process is described by $1/\lambda_{\text{in}} - 1/\lambda_p = 1/\lambda_{\text{out}}$, where $\lambda_{\text{in}} = 711$ nm is the wavelength of the input light field from the QD, $\lambda_{\text{out}} = 1313$ nm is the wavelength of the down-converted output field, and $\lambda_p = 1550$ nm is the wavelength of a strong classical pump field. InP/GaInP QDs offer the opportunity of direct electrical excitation [26] which is advantageous for operation in optical communication systems. The long-wavelength pumping scheme is chosen to minimize noise background around λ_{out} due to Raman scattering [6,11,13,15].

Figure 1(a) shows a schematic of our experimental setup which can be divided into three parts: a confocal microscope for investigation of the QD sample, a frequency conversion stage including the Zn:PPLN WG chip, and a spectral filtering stage for narrow spectral filtering of the down-converted signal. Using single photon input from a QD at a rate of $\sim 188\,400\ \text{s}^{-1}$, we measure the efficiency η_{QFC} of our frequency conversion setup as a function of the pump power P_p at 1550 nm that is coupled into the WG [Fig. 1(b)]. We define $\eta_{\text{QFC}} = \Phi_{\text{out}}/\Phi_{\text{in}}$, where Φ_{in} is the flux of visible photons at the entrance of the conversion stage and Φ_{out} is the flux of telecom photons at the output of the wavelength division multiplexer (WDM2) after the spectral filtering unit. For single photon detection at the input and output sides, we use silicon avalanche photodiodes (Si-APDs) in the visible and NbN superconducting single photon detectors (SSPDs) at telecom wavelengths,

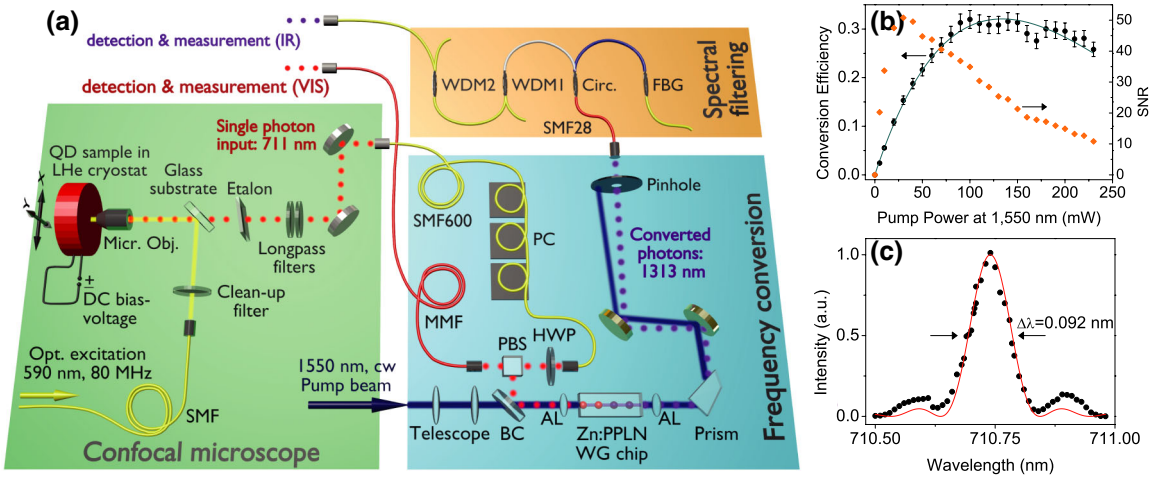

FIG. 1 (color online). Frequency down-conversion of nonclassical light emitted by a single QD. (a) Experimental setup. The confocal microscope consists of a liquid helium (LHe) continuous flow cryostat containing the QD sample at a temperature of 12 K. A bias-voltage of 3.20–3.47 V is applied to the QDs which are additionally optically excited using an average power of 160 nW at 590 nm from a pulsed fs optical parametric oscillator (OPO) with 80 MHz repetition rate [35]. Optical excitation and collection of photoluminescence (PL) emitted by a QD are performed using a 100× microscope objective with numerical aperture NA = 0.8. We collect up to 188 400 photons/s into a single-mode fiber (SMF600). A silica etalon can be inserted optionally for narrow-band filtering of the PL. Two long-pass filters prevent residual excitation light from entering the fiber. For frequency down-conversion, the visible photons are coupled into the Zn:PPLN ridge waveguide together with a strong pump beam at 1550 nm provided by a continuous-wave OPO (see the Supplemental Material [27]). The converted photons are spatially separated from the strong pump light and from residual visible photons by a prism and a pinhole and are coupled into a standard telecom fiber (SMF28). To suppress residual pump light and noise background around the target wavelength λ_{out}, we additionally use a spectral filtering setup composed of a fiber-optic circulator, a fiber Bragg grating (FBG) centered at 1312.714 nm (-1.0 dB reflection bandwidth: 0.755 nm) and two 1310 nm/1550 nm wavelength division multiplexers (WDM1 and WDM2). SMF: single mode fiber, PC: polarization control, HWP: half-wave plate, PBS: polarizing beam splitter, BC: beam combiner, AL: aspheric lens. (b) Total efficiency and SNR of the frequency conversion setup calculated from measured data using single photon input from a QD. (c) Spectral acceptance bandwidth of the DFG process measured for 2 mW input power around 710.74 nm from a tunable cw Ti:sapphire laser. For further details, see the Supplemental Material [27].

respectively (see the Supplemental Material [27]). The data are fit using $\eta_{\text{QFC}}(P_p) = \eta_{\text{QFC}}^{(\max)} \sin^2(\sqrt{\eta_{\text{nor}} P_p} L)$, where $\eta_{\text{nor}} = 115\%/(\text{W cm}^2)$ is a normalized efficiency and $L = 4$ cm is the length of the WG [3]. The point of maximum conversion is reached at $P_p = 150$ mW with $\eta_{\text{QFC}}^{(\max)} \approx 0.32$, i.e., more than 30% of the fraction of the QD emission that can be coupled into a single-mode fiber is frequency down-converted in our setup. This corresponds to an internal efficiency for photons being converted inside the WG of $\eta_{\text{int}} \gtrsim 0.64$. At the same time, the ratio of converted photons to noise photons (signal-to-noise ratio, SNR) is larger than 20:1 [Fig. 1(b)]. This unique combination of high conversion efficiency and high SNR enables faithful conversion of single photons. The internal efficiency η_{int} is ultimately limited by the nonperfect spatial overlap of the red and infrared light fields in the WG, whereas the overall efficiency η_{QFC} additionally depends on coupling and filtering losses [27]. The acceptance bandwidth of the DFG process, as seen in Fig. 1(c), is determined to be $\Delta\lambda = 0.092$ nm or $\Delta\nu = 54.6$ GHz (full width at half maximum) representing a narrow spectral bandpass filter inherent to the nonlinear process. To illustrate the effect of spectral filtering Fig. 2 shows a comparison of three photoluminescence (PL) maps along with their corresponding spectra. Figures 2(a) and 2(b) were recorded without spectral filtering. Several QDs can be identified on the map of Fig. 2(a). It is evident from the spectrum in Fig. 2(b) that a certain amount of background is still collected through the single-mode fiber. In order to select a single emission line from a single QD we insert a 56 μm-thick silica etalon (Finesse $\mathcal{F} \approx 42$, free spectral range 1.85 THz) as a narrow bandpass filter into the beam line of the visible PL light. This situation is represented in the map in Fig. 2(c) and the spectrum in Fig. 2(d). The etalon clearly suppresses PL from other QDs. The map in Fig. 2(e) was recorded by detecting converted IR-light employing a SSPD. In this case no etalon filtering of the visible input light was applied. However, from the IR-map and its related spectrum in Fig. 2(f), one recognizes that the acceptance bandwidth of the DFG process in combination with the fiber Bragg grating (FBG) represents a narrow and efficient bandpass filter with high sideband suppression. No background or further emission lines are found in the IR spectrum. Thus, for the experiments described in the following,

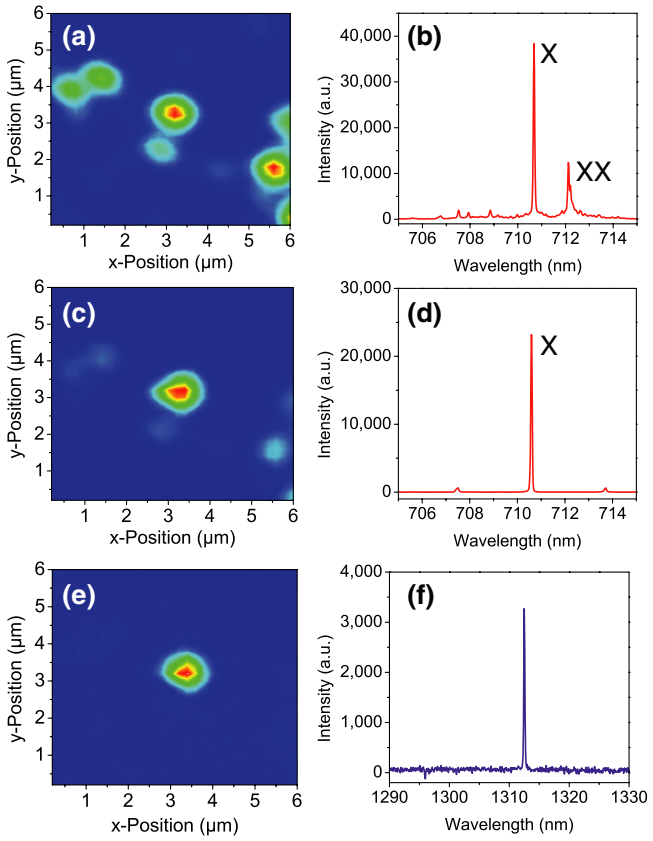

FIG. 2 (color online). PL maps with corresponding spectra. (a),(c),(e) Same 6×6 μm detail of the QD sample. Maps (a) and (c) were recorded by scanning the xy position of the sample and directly detecting the visible PL from the QD using a Si-APD (a) without and (c) with etalon filtering. Map (e) was obtained by scanning the same sample area but detecting the down-converted light at 1313 nm with a SSPD. (b),(d), (f) Spectra that were measured by setting the xy position of the sample to the point corresponding to the maximum intensity of the central QD. (b),(d) Visible PL spectrum without and with etalon filtering, respectively. The two prominent lines in (b), separated by 1.45 nm (3.54 meV), are attributed to exciton (X) and biexciton (XX) transitions. (f) Converted spectrum illustrating the effect of spectral filtering by a combination of DFG acceptance curve and FBG.

no etalon filtering was used for the telecom photons whereas the red photons were always filtered.

Many implementations of quantum communication using single photons exploit their phase coherence [19,28]. In this context, it is crucial to conserve temporal coherence during the frequency conversion process. This effect was previously measured for frequency down-conversion of weak coherent states [13]. The degree of first-order coherence of a light field is given by $g^{(1)}(\tau) = \langle \hat{E}^-(t)\hat{E}^+(t+\tau)\rangle / \langle \hat{E}^-(t)\hat{E}^+(t)\rangle$, where $\hat{E}^-(t)$ and $\hat{E}^+(t)$ are electric-field operators and τ is a time delay. We measured $g^{(1)}(\tau)$ of the single photons and determined the coherence time T_2 employing a Michelson interferometer (see the Supplemental Material [27]). The result is plotted in Fig. 3(a) for the 711 nm input photons and the 1313 nm output photons. The visibility as a function of the time delay follows an exponential decay $\exp(-|\tau|/T_2)$ as expected for a Lorentzian line shape of the QD emission. From the decay rate we find a coherence time of $T_2^{(\mathrm{vis})} = 42 \pm 17$ ps for the visible photons. Interpreting the first-order coherence as an instantaneous linewidth, i.e., as short-term frequency fluctuations, we can give a worst-case estimate of the coherence after frequency conversion: $\Delta\nu_{\mathrm{ir}} = \Delta\nu_{\mathrm{vis}} + \Delta\nu_p$, where $\Delta\nu_{\mathrm{vis}}$, $\Delta\nu_p$, and $\Delta\nu_{\mathrm{ir}}$ are the linewidth of the visible input, the pump, and the converted field, respectively. On short time scales, the linewidth of the pump light $\Delta\nu_p$ was determined to be far below 1 MHz, corresponding to a long coherence time of $T_2^{(p)} = 1/(\pi\Delta\nu_p) > 0.32$ μs. As $T_2^{(p)} \gg T_2^{(\mathrm{vis})}$ the influence of the pump light on the coherence of the converted single photons is negligible. From the coherence measurement of the converted light, we find $T_2^{(\mathrm{IR})} = 49 \pm 13$ ps. Within the measurement error, this value is in very good agreement with the coherence time of the original input photons proving conservation of the photon temporal coherence. We also measured the temporal width of the photons before and after conversion [Fig. 3(b)]. The observed decay has two contributions determined by the lifetime of the excited state of the QD and a refilling

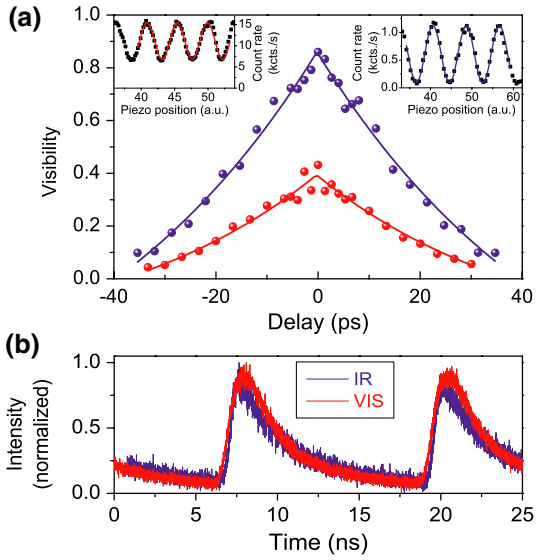

FIG. 3 (color online). Single-photon temporal coherence and lifetime before and after frequency down-conversion. (a) Visibility of first-order interference fringes vs time delay for PL from the QD at 711 nm (lower curve: data points and fit) and for converted light at 1313 nm (upper curve: data points and fit) deduced from measurements of the $g^{(1)}(\tau)$ correlation function. The insets show examples of interference fringes at fixed delay time (left inset: interference at 711 nm; right inset: interference at 1313 nm). (b) Lifetime of single photons measured via time-correlated single photon counting for original visible light and converted telecom light.

process [29]. From the data we determine the lifetime of the QD emission to be $\tau_{\mathrm{vis}} = 2.6 \pm 0.1$ ns before and $\tau_{\mathrm{IR}} = 2.9 \pm 0.4$ ns after conversion. The results agree within the error bounds, which is expected because the instantaneous conversion process should not add any temporal contribution. The much longer time constant of the refilling process in these measurements was about 2.5 μs.

We next investigate the preservation of the nonclassical single photon statistics via the degree of second-order coherence $g^{(2)}(\tau) = \langle \hat{E}^-(t)\hat{E}^-(t+\tau)\hat{E}^+(t+\tau)\hat{E}^+(t)\rangle / \langle \hat{E}^-(t)\hat{E}^+(t)\rangle^2$ using Hanbury-Brown–Twiss (HBT) interferometers [27]. Figure 4(a) shows the $g^{(2)}$-function for the light emitted by the QD. The measured $g^{(2)}_{\mathrm{vis}}(0) = 0.39 \pm 0.02 < 0.5$ for the PL of the QD clearly proves single photon emission from a single quantum emitter. A Monte Carlo simulation of the emission process reproduces the measured data very well and reveals that $g^{(2)}_{\mathrm{vis}}(0) > 0$ due to the timing jitter of the APDs (250 ps standard deviation of Gaussian envelope) and uncorrelated photon emission from background passing the etalon filter [SNR $\approx$ 7:1 determined from the spectrum of Fig. 2(d)]. For the down-converted light field, we obtain $g^{(2)}_{\mathrm{IR}}(0) = 0.24 \pm 0.04$ [see Fig. 4(b)]. The Monte Carlo simulation closely reproduces the measured data for a SNR = 12:1 of the light field and a smaller timing jitter (< 25 ps) of the SSPD, indicating that the sub-Poissonian statistics of the input light field have been fully preserved as the SNR of the QFDC process is much higher than the SNR of the light source. Even more, the SNR of the converted light is increased compared to the input light thanks to the strong spectral filtering effect of the QFDC setup. The $g^{(2)}$ cross-correlation function [Fig. 4(c)] of original and converted photons exhibits a dip as well: $g^{(2)}_{\mathrm{vis/IR}}(\tau') = 0.44 \pm 0.02$. The fact that the dip occurs at $\tau' \approx 100$ ns perfectly matches the difference of the path lengths the photons of different color have to travel to the respective detectors. The observed anticorrelation again proves the conservation of the single particle character of the light upon QFDC.

In summary, we have demonstrated efficient QFDC of visible light emitted by a true single quantum emitter to a telecom wavelength. Strong spectral filtering enables low-noise operation of the converter and a high SNR. We have experimentally proven that the temporal coherence as well as photon antibunching are conserved under frequency conversion. The converted single photons at 1313 nm (telecom O-band) are fiber coupled and the pump wavelength is at 1550 nm (telecom C-band) rendering our all-solid-state scheme fully compatible with existing telecom infrastructure. Combining a bright single quantum emitter in the visible spectral range with QFDC proves to be an elegant and flexible approach to realizing a tunable telecom-band single photon source. Concerning the implementation of quantum repeaters, we expect our experiment to work as well for input wavelengths relevant for alkali-atom-based quantum memories, e.g., 852 nm (Cs D_2 line) [30] or 795/780 nm (Rb D_1/D_2 line) [31,32]: choosing a pump wavelength between 1.9–2.1 μm allows for low-noise down-conversion to one of the telecom spectral windows. The

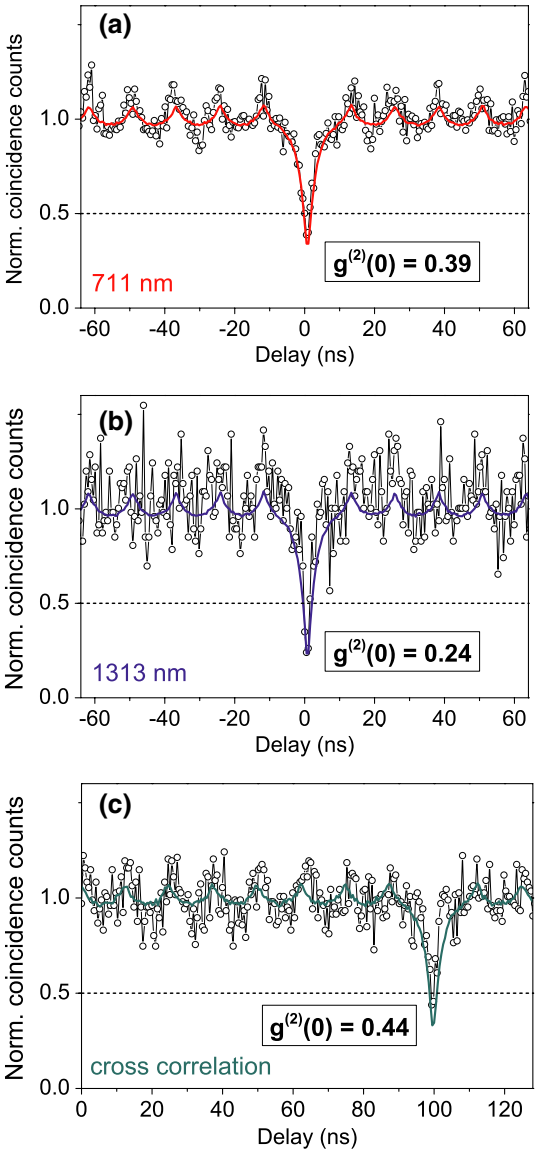

FIG. 4 (color online). Conservation of photon antibunching under frequency down-conversion: simulation and measurement. (a) $g^{(2)}$ correlation function of the single photons at 711 nm emitted by the QD (integration time $t_{\mathrm{int}} = 745$ s). (b) $g^{(2)}$ correlation function of the converted light at 1313 nm ($t_{\mathrm{int}} = 6085$ s). (c) $g^{(2)}$ cross-correlation function measured with a hybrid HBT setup, i.e., one half of the visible photons is sent directly to a visible photon detector, the other half undergoes frequency down-conversion and is then detected with an IR photon detector ($t_{\mathrm{int}} = 9440$ s). Black circles in (a)–(c) represent measured data while the solid curves are obtained from Monte Carlo simulations (see the Supplemental Material [27]). No background has been subtracted from the experimental data in all plots.

large wavelength separation in this case might require WGs with adiabatic mode size conversion [33] for high efficiency QFC. Furthermore, for many applications in long distance quantum communication QFC has to preserve the photon polarization state [7,16,34] which for our scheme can be achieved in a double-pass configuration [34].

We are indebted to Carsten Kremb for his quick help with wire bonding. We further thank Felix Rübel and Johannes L'huillier (J. L.) for lending us the fs-OPO and J. L. for helpful discussions in the early stage of the project. This work was financially supported by the Bundesministerium für Bildung und Forschung (joint project between networks QuOReP, Contract No. 01BQ1011, QuaHL-Rep, Contract No. 01BQ1041, and EphQuaM, Contract No. 01BL0902).

*christoph.becher@physik.uni-saarland.de

[1] J. Huang and P. Kumar, Phys. Rev. Lett. **68**, 2153 (1992).
[2] M. A. Albota and F. N. C. Wong, Opt. Lett. **29**, 1449 (2004).
[3] R. V. Roussev, C. Langrock, J. R. Kurz, and M. M. Fejer, Opt. Lett. **29**, 1518 (2004).
[4] S. Tanzilli, W. Tittel, M. Halder, O. Alibart, P. Baldi, N. Gisin, and H. Zbinden, Nature (London) **437**, 116 (2005).
[5] M. T. Rakher, L. Ma, O. Slattery, X. Tang, and K. Srinivasan, Nature Photon. **4**, 786 (2010).
[6] J. S. Pelc, L. Ma, C. R. Phillips, Q. Zhang, C. Langrock, O. Slattery, X. Tang, and M. M. Fejer, Opt. Express **19**, 21445 (2011).
[7] S. Ramelow, A. Fedrizzi, A. Poppe, N. K. Langford, and A. Zeilinger, Phys. Rev. A **85**, 013845 (2012).
[8] S. Ates, I. Agha, A. Gulinatti, I. Rech, M. T. Rakher, A. Badolato, and K. Srinivasan, following Letter, Phys. Rev. Lett. **109**, 147405 (2012).
[9] Z. Y. Ou, Phys. Rev. A **78**, 023819 (2008).
[10] M. W. McCutcheon, D. E. Chang, Y. Zhang, M. D. Lukin, and M. Loncar, Opt. Express **17**, 22689 (2009).
[11] H. Takesue, Phys. Rev. A **82**, 013833 (2010).
[12] J. S. Pelc, C. Langrock, Q. Zhang, and M. M. Fejer, Opt. Lett. **35**, 2804 (2010).
[13] N. Curtz, R. Thew, C. Simon, N. Gisin, and H. Zbinden, Opt. Express **18**, 22099 (2010).
[14] A. G. Radnaev, Y. O. Dudin, R. Zhao, H. H. Jen, S. D. Jenkins, A. Kuzmich, and T. A. B. Kennedy, Nature Phys. **6**, 894 (2010).
[15] S. Zaske, A. Lenhard, and C. Becher, Opt. Express **19**, 12825 (2011).
[16] R. Ikuta, Y. Kusaka, T. Kitano, H. Kato, T. Yamamoto, M. Koashi, and N. Imoto, Nature Commun. **2**, 1544 (2011).
[17] H.-J. Briegel, W. Dür, J. I. Cirac, and P. Zoller, Phys. Rev. Lett. **81**, 5932 (1998).
[18] L.-M. Duan, M. D. Lukin, J. I. Cirac, and P. Zoller, Nature (London) **414**, 413 (2001).
[19] N. Sangouard, C. Simon, H. de Riedmatten, and N. Gisin, Rev. Mod. Phys. **83**, 33 (2011).
[20] M. S. Shahriar, P. Kumar, and P. R. Hemmer, J. Phys. B **45**, 124018 (2012).
[21] B. Lauritzen, J. Minář, H. de Riedmatten, M. Afzelius, N. Sangouard, C. Simon, and N. Gisin, Phys. Rev. Lett. **104**, 080502 (2010).
[22] B. Lauritzen, J. Minář, H. de Riedmatten, M. Afzelius, and N. Gisin, Phys. Rev. A **83**, 012318 (2011).
[23] C. Simon *et al.*, Eur. Phys. J. D **58**, 1 (2010).
[24] Y. Ding and Z. Y. Ou, Opt. Lett. **35**, 2591 (2010).
[25] Y. Nishida, H. Miyazawa, M. Asobe, O. Tadanaga, and H. Suzuki, Electron. Lett. **39**, 609 (2003).
[26] M. Reischle, C. Kessler, W.-M. Schulz, M. Eichfelder, R. Roßbach, M. Jetter, and P. Michler, Appl. Phys. Lett. **97**, 143513 (2010).
[27] See Supplemental Material at http://link.aps.org/supplemental/10.1103/PhysRevLett.109.147404 for details on the quantum dot sample, experimental methods, data analysis, and numerical simulations.
[28] N. Gisin, G. Ribordy, W. Tittel, and H. Zbinden, Rev. Mod. Phys. **74**, 145 (2002).
[29] T. Aichele, V. Zwiller, and O. Benson, New J. Phys. **6**, 90 (2004).
[30] A. Kuzmich, W. P. Bowen, A. D. Boozer, A. Boca, C. W. Chou, L.-M. Duan, and H. J. Kimble, Nature (London) **423**, 731 (2003).
[31] M. D. Eisaman, A. André, F. Massou, M. Fleischhauer, A. S. Zibrov, and M. D. Lukin, Nature (London) **438**, 837 (2005).
[32] S. Ritter, C. Nölleke, C. Hahn, A. Reiserer, A. Neuzner, M. Uphoff, M. Mücke, E. Figueroa, J. Bochmann, and G. Rempe, Nature (London) **484**, 195 (2012).
[33] M. H. Chou, J. Hauden, M. A. Arbore, and M. M. Fejer, Opt. Lett. **23**, 1004 (1998).
[34] M. A. Albota, F. N. C. Wong, and J. H. Shapiro, J. Opt. Soc. Am. B **23**, 918 (2006).
[35] F. Ruebel, P. Haag, and J. A. L'huillier, Appl. Phys. Lett. **92**, 011122 (2008).